Z. Phys. Chem. **217** (2003) 975–987

Novel Ionization Mechanisms of Molecular Clusters in Ultraintense Laser Fields

By Isidore Last and Joshua Jortner*

School of Chemistry, Tel Aviv University, 69978 Tel Aviv, Israel

Dedicated to Prof. Dr. Dr. h.c. mult. Friedrich Hensel on the occasion of his 70th birthday

(Received March 4, 2003; accepted March 18, 2003)

Molecular Clusters / Ultraintense Lasers / Multielectron Ionization / Charged Nanoplasma / Femtosecond Electron Dynamics

We explore extreme multielectron ionization of $(Xe)_n$ molecular clusters resulting in the formation of highly charged Xe^{k+}, $k = 8$–32, ions in ultraintense laser fields (intensity $I = 10^{16}$–$10^{19}\,W\,cm^{-2}$), which is driven by a compound, sequential-parallel, inner-outer ionization mechanism. A computational and theoretical study is advanced for the three fundamental processes of electron fs dynamics, which involve the barrier suppression of inner ionization of the constituents, the formation of an energetic electron-positive ion charged plasma within the cluster and the outer ionization of unbound electrons from the cluster. New features of the formation, characteristics, response and dynamics of the electron-positive ion charged plasma in molecular clusters in ultraintense laser fields were explored, providing novel information on a transient (1–100 fs) metallic state in finite chemical systems.

1. Prologue

Ultraintense table top femtosecond (pulse duration ~ 100 fs) laser pulses delivering a power of ~ 10 terawats (10^{13} W) can provide an intensity of $I \sim 10^{21}\,W\,cm^{-2}$, which constitutes the highest light intensity on earth [1]. This light beam is characterized by an electric field of $\varepsilon \sim 6 \times 10^{11}\,V\,cm^{-1}$, and a magnetic field of $H \sim 10^9$ Gauss, corresponding to the largest electromagnetic fields ever produced. The interaction strength of such ultraintense light beams with matter is characterized by a Rabi frequency of $\mu\varepsilon \sim 1.2 \times 10^3$ eV (for a transition dipole moment of $\mu \sim 1$ Debye), and is expected to result in temperatures of 10^8–10^9 K, which exceed by an order of magnitude those

* Corresponding author. E-mail: jortner@chemsg1.tau.ac.il

prevailing in the interior of the sun [1, 2]. Novel features of light-matter interactions emerge from the interaction of clusters with ultrashort and ultraintense laser fields ($I = 10^{15}$–10^{20} W cm^{-2}). In general, three intensity domains for laser-matter interactions of a large, finite chemical system, *e.g.*, a large molecule or a cluster, can be distinguished [2].

(1) The 'ordinary' low intensity domain ($I < 10^{13}$ W cm^{-2}, $\mu\varepsilon < 0.1$ eV), where the electric fields of the light wave induce small oscillations of the electrons, at the same frequency, with radiative and nonradiative damping resulting in (single or multiple) photon absorption.
(2) The ultraintense intensity domain ($I = 10^{14}$–10^{19} W cm^{-2}, $\mu\varepsilon \sim 0.3$–10^2 eV), which induces strong interactions with the breakdown of perturbative quantum electrodynamics schemes, triggering ultrafast dynamics of electrons (on the time scale of < 1–10 fs) and of ions (10–100 fs time scale).
(3) The extreme ultraintense intensity domain ($I = 10^{19}$–10^{21} W cm^{-2}, $\mu\varepsilon \sim 10^2$–10^3 eV), where the electron velocities approach the velocity of light, and relativistic effects fundamentally modify the electron dynamics. In this extreme domain 'heavy electrons' with a relativistic mass of $m_e(1-(v/c)^2)^{-1/2}$ are produced and their interaction with the magnetic field of light (which is negligible in domains (1) and (2)) becomes significant [2].

Of considerable interest is the electron and nuclear dynamics of molecular clusters, *e.g.*, Xe_n, $(D_2)_n$, $(D_2O)_n$ and $(CD_4)_n$ in ultraintense ($I = 10^{14}$ -10^{19} W cm^{-2}) laser fields [3–24]. The response of large finite molecular systems, *i.e.*, clusters, to ultra-intense laser fields, is distinct both from the electron dynamics in ordinary fields ($I < 10^{13}$ W cm^{-2}) and from the response of 'small' atoms and molecules to ultraintense fields. While the ionization of single atomic and molecular systems in ultraintense laser fields is triggered by the barrier suppression single-step ionization mechanism [17], the electron dynamics of clusters in ultraintense laser fields involves three sequential-parallel processes:

(1) Inner ionization [16–19], which involves the stripping of the cluster atoms of some of their electrons, of all their valence electrons or of all their electrons, with the inner ionization level being mainly determined by the electronic structure of the atoms and by the laser intensity.
(2) Formation of an energetic electron-positive ion charged plasma within the cluster (or in its vicinity), which consists of unbound electrons interacting with the ultraintense laser field.
(3) Outer ionization [17, 20], which removes all or part of the unbound electrons of the energetic charged plasma from the cluster.

Of course, these three electronic processes are coupled to each other. The overall cluster ionization process is initiated by inner ionization and plasma

formation, with outer ionization of the plasma usually occurring on a longer time scale than inner ionization. The separation of (fs) time scales for inner ionization + plasma formation and of outer ionization is intensity dependent. The electronic dynamic processes trigger nuclear dynamics, with outer ionization being accompanied by cluster Coulomb explosion [3–24], which results in the production of energetic (keV–MeV) multicharged ions. Generally speaking, the electronic processes and the nuclear process of Coulomb explosion are hierarchical. In the laser intensity domain of $I > 10^{18}\ \mathrm{W\,cm^{-2}}$ the electronic and nuclear processes can be decoupled, separating time scales for fast (fs) electron dynamics and for (10–100 fs) nuclear Coulomb explosion. The hierarchy of the electron and nuclear dynamics is summarized in Scheme 1.

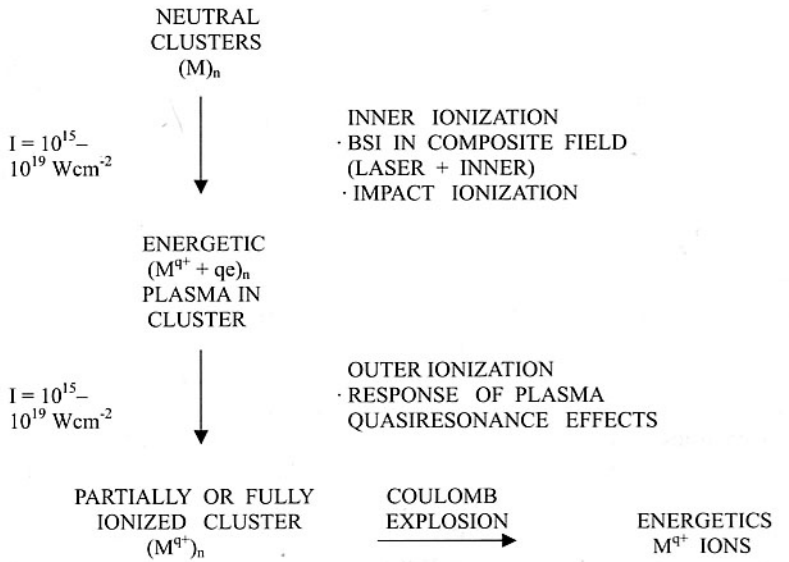

Scheme 1. Electron and nuclear dynamics of molecular clusters in ultraintense laser fields. Inner ionization is induced by the barrier supression ionization (BSI) mechanism with a minor contribution from impact ionization. Outer ionization is induced by laser-plasma interaction.

In this paper we explore some new features of electron dynamics in elemental $(Xe)_n$ ($n = 55$–1061) clusters responding to ultraintense laser fields ($I = 10^{16}$–$10^{18}\ \mathrm{W\,cm^{-2}}$). Extreme cluster multielectron ionization is accomplished with the formation of highly charged Xe^{k+} ($k = 8 - 32$) ions, in accord with some experimental data [4, 5, 25]. The novel features of cluster (distinct from single atom) inner/outer ionization will be explored by nonrelativistic molecular dynamics simulations. Of considerable interest are the properties and response of the nonequilibrium charged plasma produced in the inner ion-

ization in the elemental cluster and depleted by quasiresonance interactions with the laser field. The characteristics of the charged plasma in a cluster (a 'nanoplasma') are of considerable interest and previously attracted considerable interest [26]. Our molecular dynamics simulations are expected to provide new information on the formation and ionization of the plasma in ultraintense laser fields.

2. Simulations and estimates

Extreme multielectron ionization of $(Xe)_n$ ($n = 55 - 1061$) clusters in ultraintense ($I = 10^{16}$–10^{18} W cm^{-2}) laser fields (whose maximal electric field value is $eF_m = 2.75 \times 10^{-7} I^{1/2}$ eV Å^{-1}) was treated by the simulation methods previously described by us [17, 20–22]. The laser electric field was taken as $F_\ell(t) = F_{\ell 0}(t)\cos(2\pi\nu t + \varphi_0)$ with the frequency $\nu = 0.35$ fs^{-1} (photon energy 1.44 eV). The field envelope was described by a truncated Gaussian $F_{\ell 0}(t) = F_m \exp[-2.77(t/\tau - \kappa)^2]$, with a half linewidth of $\tau = 25$ fs, and an onset (at $t = 0$) of $F_{\ell 0}(0) = 0.5\, F_m$ (for $\kappa = 0.5$). The ionization of the constituent atoms in the strong electromagnetic field, whose photon energy (1.44 eV) is considerably lower than the Xe^{k+} ionization potentials, was treated by the classical barrier suppression ionization (BSI) mechanism [28] triggered by a composite electric field consisting of the laser + internal cluster field, which results in the inner ionization process. The classical approach was also applied to the energetics and dynamics of the unbound, high-energy electrons inside and outside the cluster. The heavy Xe^{k+} ions were treated as classical particles. The simulations of the electron dynamics of the energetic charged plasma and of the outer ionizations and the nuclear dynamics of the ions were carried out, using a potential involving ion–electron, electron–electron and laser–charge interactions. The integration of the classical equations of motion was conducted using attosecond time steps (*i.e.*, 1 attosend for electrons and 20–40 attoseconds for ions) which were applied for electron–nuclear dynamics in the time scale of 1–100 fs.

Inner ionization of a single k-fold charged atomic ion via the BSI mechanism is realized when the effective electric field F (laser field F_ℓ + inner field) satisfies the relation [17] $|eF| > P_k^2/4B(k+1)$, where P_k is the ionization potential of the ion [28] and $B = 14.39$ eV. When this condition is fulfilled, the inner ionization event is manifested by locating the removed electron at the barrier distance [17] $x_b = [B(k+1)/eF]^{-1/2}$ from the centre of the atom with zero kinetic energy. The multielectron ionization of each atom is realized sequentially, with each electron being removed at an attosecond time step. The electrons released by inner ionization respond to the laser field, gain energy in the 10 eV – 1 k eV domain, and also interact with the ions triggering a small contribution ($\lesssim 10\%$ yield for clusters with $n < 1000$) of collision-induced ionization [15, 27], which further contributes to the inner ionization

process. The outer ionization event involving the removal of an electron from the plasma within the cluster was recorded when the distance of this electron from the cluster center was taken (arbitrarily) to be more than six times larger than the Coulomb expanding cluster radius of the nuclear framework. Two comments regarding these simulations are in order. First, since all the electrostatic ion–ion, ion–electron and electron–electron interactions are included explicitly in our simulations, the effects of hydrodynamic pressure [4, 6] on the electron and ion dynamics associated with the high energy electrons seems to have been taken into account. Second, the laser–electron and laser–ion interactions, which are included in our simulations, seem to account properly for resonance absorption effects by the plasma [26] in the high intensity domain.

3. Mechanistic facets of cluster ionization

We first consider multielectron ionization of a single Xe atom, whose ionization potentials of Xe^{k+} ions are known [28]. Following the analysis of Sect. 2 (with $F = F_m$), some representative results for the ionization levels of Xe^{k+} ions are: $k = 8$ for $I = 10^{16}\,\mathrm{W\,cm^{-2}}$, $k = 14$ for $I = 10^{17}\,\mathrm{W\,cm^{-2}}$, $k = 18$ for $I = 10^{18}\,\mathrm{W\,cm^{-2}}$ and $k = 32$ for $I = 10^{19}\,\mathrm{W\,cm^{-2}}$. The BSI model predictions for multielectron ionization of a single Xe are in accord with experimental data [29, 30], which reveal the formation of Xe^{+8} ions at $I \simeq 0.6 \times 10^{16}\,\mathrm{W\,cm^{-2}}$ and the generations of Xe^{+20} ions at $I = 10^{18}\,\mathrm{W\,cm^{-2}}$. The ionization level of a (single-step) multielectron ionization of a single many-electron atom or molecule involves the suppression of the electrostatic barrier produced by the laser field. The marked increase of the single-atom ionization level with increasing the laser intensity manifests the enhancement of the ionization of inner electronic shells.

Cluster multielectron intense-field ionization is distinct from that of a single atom. The mechanistic differences pertain to:

(1) Compound, multistep cluster ionization involving sequential-parallel, inner-outer ionization mechanisms. For the onset of the compound cluster ionization mechanism, the lower limit of the cluster size sets in when the cluster radius R significantly exceeds the (single species) barrier distance x_b, *i.e.*, $R \gg x_b$.
(2) Distinct time scales for cluster inner ionization, prevalence of the charged plasma and outer ionization (scheme 1) can be distinguished
(3) The cluster inner ionization is driven by a composite electric field $\boldsymbol{F} = \boldsymbol{F}_\ell + \boldsymbol{F}_i$ consisting of the laser field $\boldsymbol{F}_\ell$ and the inner field $\boldsymbol{F}_i$, which is generated by the ions and the unbound electrons. Each of the cluster ions undergoes BSI induced by the composite field.
(4) Two major effects of the inner field on the cluster inner ionization level are: (i) The ignition mechanism. In a highly positively charged cluster the

increase of the inner field enhances the inner ionization level; (ii) The screening mechanism. This is manifested when the number of unbound electrons in the cluster is large, providing a screening effect which weakens the laser field and attenuates the inner ionization level.

(5) The inner ionization process results in a charged plasma in the cluster, while the subsequent removal of electrons from the plasma induced by the composite field constitutes the outer ionization process.

(6) The mechanism of cluster outer ionization involves both static laser field effects, *i.e.*, BSI of the entire cluster as well as dynamic quasiresonance effects (Sect. 5).

4. Cluster inner and outer ionization – ionization levels and electron dynamics

In Xe_n clusters, the Xe^{k+} inner ionization level increases with increasing the laser intensity at a constant cluster size, and increases with increasing the cluster size at a fixed intensity, revealing the effects of field ionization, ignition enhancement and screening effects. These features are manifested by the time dependence of the ionization level obtained from the numerical simulations (Fig. 1). For $(Xe)_{459}$ the highest values of the average inner ionization level, k_{av}, are $k_{av} = 7.3$ at $I = 10^{16}\ W\,cm^{-2}$ and $k_{av} = 20.9$ at $I = 10^{18}\ W\,cm^{-2}$ (Fig. 1), with the marked increase of k_{av} with increasing I reflecting the appreciable enhancement of the field ionization at high intensities. The cluster size dependence of the inner ionization level at high intensities is reflected at $I = 10^{18}\ W\,cm^{-2}$, where $k_{av} = 20.9$ for $(Xe)_{459}$ and $k_{av} = 22.7$ for $(Xe)_{1061}$. The cluster size dependence of the ionization levels is portrayed in Fig. 2, where the increase of both the average level, k_{av}, and the maximal level, k_{mx}, with increasing the cluster size at the ultrahigh intensity $I = 10^{18}\ W\,cm^{-2}$ is due to the ingition effect. The manifestation of the cluster ignition effect (Fig. 2) is clearly exhibited for the values of k_{mx} and k_{av} for Xe_n ($n = 55 - 1061$) clusters at $I = 10^{18}\ W\,cm^{-2}$, exceeding the ionization level of a single atom, which is also marked on Fig. 2. A qualitatively similar ignition effect is also manifested for k_{mx} at the lower intensity of $I = 10^{16}\ W\,cm^{-2}$ (Fig. 2), however, here the slight decrease of k_{av} with increasing n is due to superposition of ignition and screening effects in the inhomogeneous distribution of the Xe^{k+} ions. In an attempt to confront our simulation results for the inner ionization level with the available experimental results [25], we consider the high I domain where the asymptotic value of k_{mx} for inner ionization is equal to that of the outer ionization (Fig. 1). The simulated data for $(Xe)_{1061}$ at $I = 1061$ give $k_{mx} = 26$, being close to the experimental maximal charges of $k = 25$–30 reported [25] for very large $(Xe)_n$ ($n = 2 \times 10^6$) clusters at $I = 5 \times 10^{17}\ W\,cm^{-2}$. What is interesting is the generation of very high ionic charges ($k \sim 26$) by cluster multielectron, ultraintense laser field ($I = 10^{18}\ W\,cm^{-2}$) ionization.

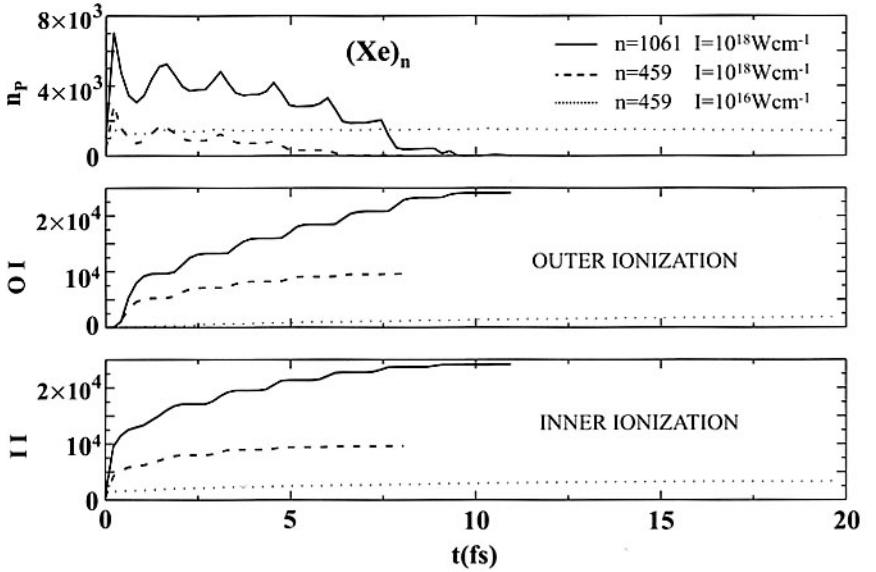

Fig. 1. Time-resolved electron dynamics in $(Xe)_n$ ($n = 459$ and 1061) clusters in ultraintense laser fields ($I = 10^{16}$ and 10^{18} W cm^{-2}). The n and I data are marked on the figures. The laser electric field (Sect. 2) was taken as a truncated Gaussian envelope $F_{t0}(t) = F_m \exp[-2.77(t/\tau - 0.5)^2]$. The lower panel portrays the cluster inner ionization (II) levels F (total number of unbound electrons generated by inner ionization), the middle panel gives the cluster outer ionization (OI) levels (number of unbound electrons removed from the cluster by outer ionization), and the top panel represents the total number of electrons (n_P) in the nonequilibrium charged plasma.

The charged plasma produced by inner ionization interacts with the effective (laser + inner) field, which results in the outer ionization process. Energy pumping from the laser field to the unbound electrons can be enhanced by the quasiresonance mechanism, which is accompanied by the outer cluster ionization. Some novel features of inner/outer ionization dynamics emerge from our simulations (Fig. 1 and Table 1). The time scales (defined as the half lifetimes for the accomplishment of half of the asymptotic ionization level) for inner ionization ($\tau^{(i)}$) and for outer ionization ($\tau^{(o)}$) are in the fs-subfs time domain (Table 1) with a clear indication of sequential electron dynamics. In the intensity domain $I = 10^{16}$–10^{18} W cm^{-2} the inner/outer ionization processes are sequential (Fig. 1). These sequential characteristics become prominent at the lower intensities of $I = 10^{16}$ W cm^{-2} ($\tau^{(i)} = 0.5$ fs, $\tau^{(o)} = 2$ fs) and also for the large clusters of $n = 1061$ ($\tau^{(i)} = 0.5$ fs and $\tau^{(o)} = 2$ fs) at $I = 10^{18}$ W cm^{-2}. We note that the subfs time scales ($\tau^{(i)}$) for inner ionization depend on the truncated Gaussian envelope shape chosen for the electric field (Sect. 2), constituting a lower limit for the time scale of this electronic process. These time scales for the coupled electron–laser

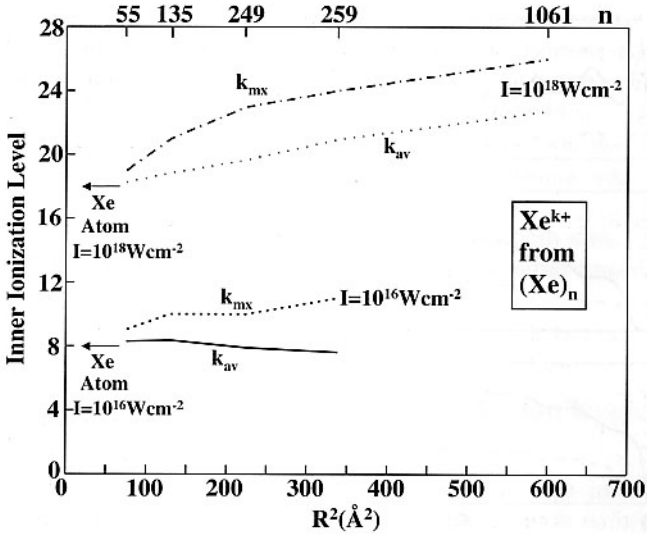

Fig. 2. Cluster size and laser intensity dependence of the average (k_{av}) and maximal (k_{mx}) inner ionization level of Xe^{k+} ions from $(Xe)_n$ clusters ($n = 55$–1061). Intensities are marked on the curve. At a high intensity of $I = 10^{18}$ W cm^{-2} the increase of the inner ionization level with increasing the cluster size is due to the inner field ignition effects. The ionization levels of a single Xe atom are marked by arrows.

Table 1. Time-resolved dynamics of inner/outer ionization of $(Xe)_n$ clusters ($\tau^{(i)}$ – lifetime for inner ionization, $\tau^{(o)}$ – lifetime for outer ionization), average plasma electron energies (ϵ_{av}) and maximal number n_P of electrons per Xe atom at time (t) in the plasma.

n	I (W cm^{-2})	$\tau^{(i)}$ (fs)	$\tau^{(o)}$ (fs)	ϵ_{av} (eV)	n_P
459	10^{16}	0.5	10	10–50	3.2 (20–50 fs)
459	10^{18}	0.3	0.4	150–1300	3.6 (1.6 fs)
1061	10^{18}	0.5	2	300–2500	4.9 (2.9 fs)

processes depend on the pulse shape of the laser (Sect. 2) which was used herein.

The electron population n_P of the plasma per Xe atom (Table 1) is finite over a 'long' time scale at $I = 10^{16}$ W cm^{-2}, where $n_P = 3.2$ for 20–50 fs (Fig. 1), while at higher intensities of $I = 10^{18}$ W cm^{-2} the plasma is depleted on the time scale of < 10 fs (Fig. 1). The energetics of the electrons in the high-energy plasma is specified in terms of their average energies (Table 1), which exhibit a marked cluster size dependence at a fixed intensity, *i.e.*, at $I = 10^{18}$ W cm^{-2}. The energies are 150–1300 eV for $n = 459$ and 300–2500 eV

for $n = 1061$ and increase with increasing intensity (*i.e.*, for $n = 459$, the average electron energies are 10–50 eV at $I = 10^{16}$ W cm^{-2} and 150–1300 eV at $I = 10^{18}$ W cm^{-2}). The response of this high-energy plasma to the laser field provides the basis for the outer ionization process.

5. The charged plasma

The properties and response of the high-energy charged plasma produced via inner ionization within the molecular cluster is of interest. These clusters, which contain the plasma, are highly positively charged with the lowest values of the excess positive charge per Xe atom being $Q = (k_{av} - n_p)$. For $(Xe)_{459}$ at the lower intensity domain of $I = 10^{16}$ W cm^{-2}, $n_p = 3.2$ and $Q = 4.1$ over the 'long' time domain of 20–50 fs (Table 1 and Fig. 1). At these 'long' times ($\gtrsim 20$ fs) and lower intensities ($I = 10^{16}$ W cm^{-2}) the outer ionization process is incomplete and the electron cloud is retained in the cluster. During the 'long' time domain, the multicharged cluster undergoes Coulomb explosion. These interesting nuclear dynamics phenomena, which recently provided a path for nuclear fusion induced by cluster Coulomb explosion [11, 12, 22–24, 31], will not be considered in the present paper, which focuses on electron dynamics. On the other hand, for $(Xe)_{459}$ at the high intensity (10^{18} W cm^{-2}), $Q = 17.3$ at $t = 1.6$ fs, while at long times ($t \gtrsim 10$ fs) the $(Xe)_n$ ($n = 459$, 1061) outer ionization process is nearly complete (Fig. 1) with $n_p = 0$ and $Q = k_{av}$. We conclude that the energetic charged plasma can be sustained on the longer time scale of tens of fs ($\lesssim 50$ fs) in the lower intensity domain of $I = 10^{16}$ W cm^{-2} and on the fs (1–3 fs) time scale at higher ($I = 10^{18}$ W cm^{-2}) intensities.

In the clusters studied herein, the maximal number, $n_p \simeq 3$–5, of electrons per Xe atom (Table 1) can be used to estimate the electron density $N_p = n_p/(4\pi/3)(R_{Xe})^3$, where n_p data are given in Table 1 and $R_{Xe} = 3.3$ Å is the radius of a Xe atom, which results in the values of $N_p = (2.0–4.0) \times 10^{22}$ cm^{-3}. These electron densities in highly ionized molecular clusters are comparable to electron densities in a metal. The lifetime of these high electron densities is determined by the laser intensity dependent outer ionization time.

Regarding the response of the plasma to the laser field, it was proposed [26] that when the natural frequency ω_p of the plasma equals the laser frequency, resonance absorption in the cluster may occur, which may provide a mechanism for energy pumping into the cluster and for outer ionization. In the bulk plasma a resonance will be manifested at $\omega_p^B = (4\pi e^2 N_p/m_e)^{1/2}$, while for a cluster (with a radius considerably smaller than the wavelength of light) the plasma frequency is $\omega_p = (4\pi e^2 N_p/3m_e)^{1/2}$. From the estimate of the range of the N_p values given above, we estimate the plasma frequencies $\omega_p = (4.6–7.0) \times 10^{15}$ s^{-1}, being close to that of a many-electron metal, with the characteristic plasma energies of $\hbar\omega_p = 3$–5 eV. A validity condition for

the simple picture of the collective plasma oscillations with the frequency ω_p is [32] $\omega_p^2 \gtrsim 2k^2 \epsilon_{av}/3m_e$, where $k = 2\pi/\lambda_e$ is the wave vector of the space charge oscillations and ϵ_{av}= 10–50 eV is the electron kinetic energy for the lower intensity domain (Table 1). A further study of these collective plasma oscillations will be of interest. The simple estimate of $\omega_p = 3$–5 eV given above exceeds the photon energies (1.44 eV) used in the present simulations, precluding resonance absorption. Furthermore, at the high intensities considered herein, a linear response of the plasma to the laser field is not feasible.

The response of the charged plasma to the ultraintense laser fields is enhanced by quasi-resonance effects. The motion of the highly mobile electrons inside the cluster is roughly in phase with the laser field. This is manifested for $(Xe)_{459}$ at lower intensities of $I = 10^{16}$ W cm^{-2}, where the electron cloud undergoes an oscillatory time-dependent distribution in the oscillating laser field (Fig. 3). At this lower intensity domain ($I = 10^{16}$ W cm^{-2}) the plasma survives for a moderately long ($\gtrsim 50$ fs) time and is confined in the cluster. On the other hand, for the response of the plasma at very high intensities ($I = 10^{18}$ W cm^{-2}) the unbound electrons mostly move outside the cluster (Fig. 4). The unbound electrons outside the cluster move along the laser field polarization direction (the x axis in Fig. 4), forming an elongated cloud along this direction.

Some manifestations of quasiresonance effects are of interest. Both inner and outer ionization processes in $(Xe)_n$ clusters at high intensities ($I = 10^{18}$ W cm^{-2}) exhibit weak oscillations (Fig. 1) with a frequency that is twice as large as the laser frequency. The maxima of the temporal oscillations in the inner ionization level and of n_p coincide with the laser field (Fig. 1), in accord with the physical model of field ionization of the constituents (Sects. 2 and 4). The temporal oscillations for the outer ionization yield curves (Fig. 1) are shifted in phase with respect to the oscillations of the laser field.

6. Concluding remarks

Extreme cluster multielectron ionization in ultraintense laser fields is a novel and interesting research area. It is distinct from that of a single atom or molecule ionization in terms of mechanisms, nature of the intermediate plasma state, characteristics of ionic products, and time scales for electron and nuclear dynamics. Several novel features emerge from our study. (1) A novel cluster ionization mechanism. When the cluster size (or that of a large chemical system) significantly exceeds the size of the constituent barrier distance, *i.e.*, $x_b \ll R$ (Sects. 2 and 3), a compound cluster ionization mechanism is manifested, which occurs via sequential-simultaneous, inner-outer ionization. (2) Methodology. Simulation methods for the study of the interaction of large, finite chemical systems, *i.e.*, clusters or molecules, with ultraintense laser fields

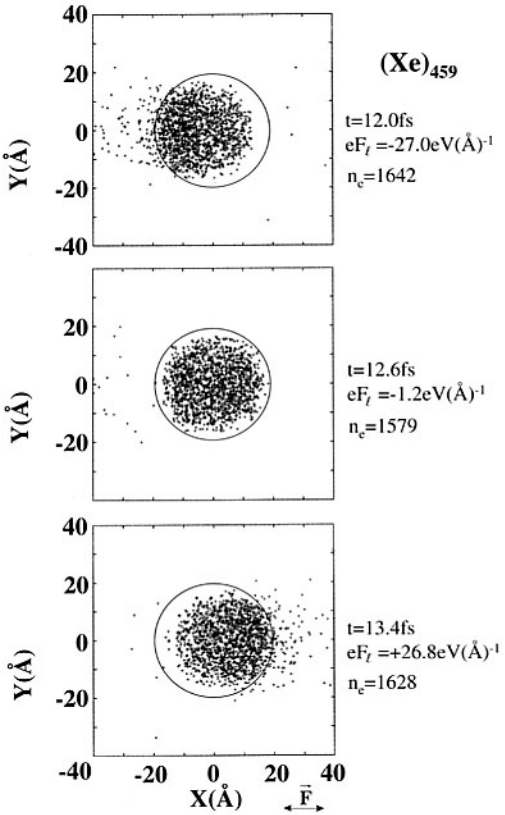

Fig. 3. The dynamics of the electron cloud (represented in two dimensions) in a $(Xe)_{459}$ cluster driven by a laser field (specified in Sect. 2) corresponding to an intensity of $I = 10^{16}\,\mathrm{W\,cm^{-2}}$. The laser is polarized across the x axis and the propagation direction is along the z axis. The times (t) are measured relative to the onset $t = 0$ of the laser pulse (for $\kappa = 0.5$) and the laser field $F_\ell(t)$ is given in eV Å^{-1}. The crosses represent the electrons, while the circles represent the cluster size. The plasma oscillates in the laser field exhibit a left-side/right-side biased distribution at $t = 12$ fs/13.4 fs when $eF_\ell = -27.2$ eV Å^{-1}/26.8 eV Å^{-1} and a central distribution at $t = 12.6$ fs at a low $eF_\ell = -1.2$ eV Å value.

were utilized. (3) Ultrafast electron dynamics (< 1–10 fs). Ultrafast cluster dynamics is not only limited to the exploration of dynamics of ions on the time scale of nuclear motion, but is extended to the new realm of electron dynamics. (4) The non-equilibrium, nanoplasma. The formation, characteristics, response and dynamics of an energetic electron–positive ion charged plasma in molecular clusters in ultraintense laser fields were explored, providing novel information on a transient (1–100 fs) metallic state in a large, finite, molecular system.

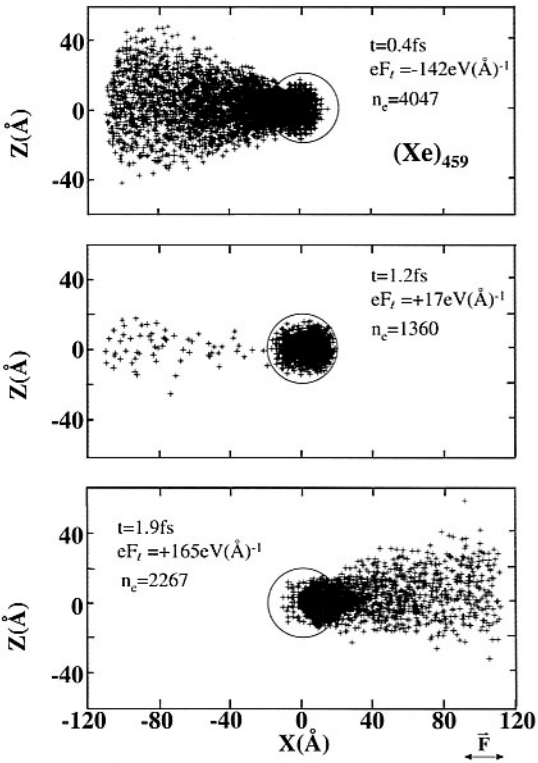

Fig. 4. The dynamics of the electron cloud in $(Xe)_{459}$ clusters at the intensity of $I = 10^{18}$ W cm^{-2}. Laser field characteristics and notation as in Fig. 3. The simulations represent oscillatory time dependence of the electron cloud driven by the laser field, manifesting a left-side/right-side biased distribution at large $|eF_t|$ values and a central distribution for low $|eF_t|$.

Acknowledgement

This research was supported by the German–Israeli Binational James Franck Program on Laser–Matter Interactions.

References

1. G. A. Mourou, C. P. J. Barty, and M. D. Perry, Phys. Today **51** (1998) 22.
2. G. A. Mourou and D. Umstadter, Sci. Am. **63** (May 2002).
3. E. M. Snyder, S. Wei, J. Purnell, S. A. Buzza, and A. W. Castleman, Jr., Chem. Phys. Lett. **248** (1996) 1.
4. T. Ditmire, J. W. G. Tisch, E. Springate, M. B. Mason, N. Hay, R. A. Smith, J. Marangos, and M. H. R. Hutchinson, Nature **386**(6) (1997) 54.
5. K. Kondo, A. B. Borisov, C. Jordan, A. McPherson, W. A. Schroeder, K. Boyer, and C. K. Rhodes, J. Phys. B **30** (1997) 2707.

6. T. Ditmire, E. Springate, J. W. G. Tisch, Y. L. Shao, M. B. Mason, N. Hay, J. P. Marangos, and M. H. R. Hutchinson, Phys. Rev. A **57** (1998) 369.
7. J. V. Ford, O. Zhong, L. Poth, and A. W. Castleman, Jr., J. Chem. Phys. **110** (1999) 6257.
8. L. Köller, M. Schumacher, J. Köhn, J. Tiggesbäumker, and K. H. Meiwes-Broer, Phys. Rev. Lett. **82** (1999) 3783.
9. M. Lezius, V. Blanchet, D. M. Rayner, D. M. Villeneuve, A. Stolov, and M. Yu. Ivanov, Phys. Rev. Lett. **86** (2001) 51.
10. E. Springate, N. Hay, J. W. G. Tisch, M. B. Mason, T. Ditmire, M. H. R. Hutchinson, and J. P. Marangos, Phys. Rev. A **57** (2000) 063201.
11. J. Zweiback, R. A. Smith, T. E. Cowan, G. Hays, K. B. Wharton, V. P. Yanovsky, and T. Ditmire, Phys. Rev. Lett. **84** (2000) 2634.
12. J. Zweiback, T. E. Cowan, R. A. Smith, J. H. Hurtlay, R. Howell, C. A. Steinke, G. Hays, K. B. Wharton, J. K. Krane, and T. Ditmire, Phys. Rev. Lett. **85** (2000) 3640.
13. S. Teuber, T. Töppner, T. Fennel, J. Tiggesbäumker, and K. H. Meiwes-Broer, Eur. Phys. J. D **16** (2001) 59.
14. V. Kumarappan, M. Krishnamurthy, D. Mathur, and L. C. Tribedy, Phys. Rev. A **63** (2001) 023203.
15. D. A. Card, E. S. Wisniewski, D. E. Folmer, and A. W. Castleman, Jr., J. Chem. Phys. **116** (2002) 3554.
16. T. Ditmire, Phys. Rev. A **57** (1998) R4094.
17. I. Last and J. Jortner, Phys. Rev. A **62** (2000) 013201.
18. K. Ishikava and T. Blenski, Phys. Rev. A **62** (2000) 063204.
19. V. P. Krainov and A. S. Roshchupkin, Phys. Rev. A **64** (2001) 063204.
20. I. Last and J. Jortner, Phys. Rev. A **60** (1999) 2215.
21. I. Last and J. Jortner, Phys. Rev. **64** (2001) 063201.
22. I. Last and J. Jortner, Phys. Rev. Lett. **87** (2001) 033401.
23. P. B. Parks, T. E. Cowan, R. B. Stephens, and E. M. Campbell, Phys. Rev. **63** (2001) 063203.
24. I. Last and J. Jortner, Chem. Phys. Chem. **3** (2002) 845.
25. M. Lezius, S. Dobosh, D. Normand, and M. Schmidt, Phys. Rev. Lett. **80** (1998) 261.
26. J. Zweiback, T. Ditmire, and M. D. Perry, Phys. Rev. A **59** (1999) R3166.
27. W. Lotz, Z. Phys. **216** (1968) 241.
28. S. Augst, D. Strickland, D. D. Meyerhofer, S. L. Chin, and J. Eberly, Phys. Rev. Lett. **63** (1989) 2212.
29. G. Gibson, T. S. Luk, and C. K. Rhodes, Phys. Rev. A **41** (1990) 5049.
30. M. Dammasch, M. Dörr, U. Eichmann, E. Lenz, and W. Sandner, Phys. Rev. **64** (2001) 061402R.
31. G. Grillon, Ph. Balcou, J.-P. Chambaret, D. Hulin, J. Martino, S. Moustaizis, L. Notebaert, M. Pittman, Th. Pussieux, A. Rousse, J.-Ph. Rousseau, S. Sebban, O. Sublemontier, and M. Schmidt, Phys. Rev. Lett. **89** (2002) 065005-1.
32. R. Kubo and T. Nagamiya, *Solid State Physics*, McGraw Hill, New York (1969), pp. 112–119.